

---

This is an electronic reprint of the original article.  
This reprint may differ from the original in pagination and typographic detail.

Rautiainen, Matti; Remes, Heikki; Niemelä, Ari; Romanoff, Jani

## Fatigue strength assessment of complex welded structures with severe force concentrations along a weld seam

*Published in:*  
International Journal of Fatigue

*DOI:*  
[10.1016/j.ijfatigue.2022.107321](https://doi.org/10.1016/j.ijfatigue.2022.107321)

Published: 01/02/2023

*Document Version*  
Publisher's PDF, also known as Version of record

*Published under the following license:*  
CC BY

*Please cite the original version:*  
Rautiainen, M., Remes, H., Niemelä, A., & Romanoff, J. (2023). Fatigue strength assessment of complex welded structures with severe force concentrations along a weld seam. *International Journal of Fatigue*, 167, Article 107321. <https://doi.org/10.1016/j.ijfatigue.2022.107321>

---

This material is protected by copyright and other intellectual property rights, and duplication or sale of all or part of any of the repository collections is not permitted, except that material may be duplicated by you for your research use or educational purposes in electronic or print form. You must obtain permission for any other use. Electronic or print copies may not be offered, whether for sale or otherwise to anyone who is not an authorised user.



# Fatigue strength assessment of complex welded structures with severe force concentrations along a weld seam

Matti Rautiainen<sup>a,b,\*</sup>, Heikki Remes<sup>a</sup>, Ari Niemelä<sup>b</sup>, Jani Romanoff<sup>a</sup>

<sup>a</sup> Department of Mechanical Engineering, Aalto University School of Engineering, P.O. Box 15300, 02150 Espoo, Finland

<sup>b</sup> Structural Design, Meyer Turku Oy, Telakkakatu, 1, 20101 Turku, Finland

## ARTICLE INFO

### Keywords:

Fatigue  
Welded joint  
Full-scale test  
Weld root

## ABSTRACT

This paper investigates weld root fatigue strength of complex structures including severe force concentrations along a weld seam. Fatigue tests were carried out for a pillar assembly with various weld configurations. A comparative analysis was carried out with local nominal weld stress (LNWS), structural weld stress, and effective notch stress (ENS) approaches. The study shows that the LNWS approach gives the best prediction, with a scatter range index of 1.26 to 1.68 depending on the weld type. The accuracy of the structural weld stress approach and ENS was significantly lower, with a scatter range index of 4.98 and 5.40, respectively.

## 1. Introduction

Large thin-walled structures include complex welded connections such as tubular joints in offshore or steel bridge structures [1,2] and cruciform connections in ships [3]. The common feature of these complex connections is structural discontinuity resulting from unsymmetrical connections, differences in plate thickness, partially penetrated fillet welds, and one-sided welding. These structural discontinuities result in severe stress concentration at the weld root, and this stress concentration can have significant variation along a single weld seam. The latter is called a weld force concentration since it is due to the variation of the load-carrying mechanism of the structural assembly. These structural complexities make the fatigue analysis of such connections extremely challenging. An example of the complex stress distribution on the RHS pillar connection on a cruise ship is shown in Fig. 1. For weld root analysis the most common approaches are the nominal weld stress approach, local nominal weld stress approach (LNWS), structural weld stress approach, and effective notch stress approach (ENS), for which the definitions are listed in Table 1 [4]. In design codes, for nominal weld stress approaches the FAT class varies according to the weld type, whereas for structural weld stress and ENS a fixed FAT class independent of the weld type is used.

In the nominal weld stress approach the stress  $\sigma_w$  is calculated by

dividing the weld force  $F$  by the total weld throat cross-section area, i.e. the product of the weld throat thickness  $a_w$  and seam length  $L$  for all welds giving

$$\sigma_w = \frac{F}{\sum a_w L} \quad (1)$$

This nominal weld stress and the corresponding FAT class do not contain information about weld force concentrations and thus this approach is best suited to 2D structures, where the load is distributed equally along the whole length of the weld seam. In fatigue design rules and recommendations, a FAT class of 36–45 is used, depending on the weld throat thickness, plate thickness, and connection type [5–7].

By using a local nominal weld stress approach (LNWS), the force concentration is included as the nominal stress is calculated by dividing the local weld force value by the weld throat thickness. Recently, it has been demonstrated by Rautiainen et al. [8] that an LNWS approach improves the accuracy of the fatigue assessment significantly compared to the weld nominal stress approach when applied to 3D structures with weld force concentrations. The local nominal weld stress is defined on the basis of the load distribution obtained from FE modelling and based on the fatigue class FAT36-40. However, very few papers can be found for fatigue assessment with an LNWS approach and only rather simple fillet welded connections have been presented [9]. Therefore, it remains unclear if a similar fatigue class is valid for more complex connections

*Abbreviations:* DC, Displacement controlled test; DFW, Double fillet weld; ENS, Effective notch stress; FB, Flat bar; FC, Force-controlled test; FCF, Force concentration factor; FE, Finite element; FW, Fillet weld; LNWS, Local nominal weld stress; RHS, Rectangular hollow section; SSPPFW, Single-sided partially penetrated fillet weld; MAG, Metal active gas; PP, Partial penetration weld.

\* Corresponding author.

*E-mail address:* [matti.rautiainen@aalto.fi](mailto:matti.rautiainen@aalto.fi) (M. Rautiainen).

<https://doi.org/10.1016/j.ijfatigue.2022.107321>

Received 3 July 2022; Received in revised form 13 September 2022; Accepted 6 October 2022

Available online 12 October 2022

0142-1123/© 2022 The Author(s). Published by Elsevier Ltd. This is an open access article under the CC BY license (<http://creativecommons.org/licenses/by/4.0/>).

Nomenclature	
$a_w$	Weld throat thickness [mm]
$F$	Weld force [N]
$f_l$	Line force [N/mm]
$h$	Weld leg height [mm]
$K_t$	Stress concentration factor [-]
$L$	Weld length [mm]
$l$	Weld leg length [mm]
$m$	Negative inverse slope of S—N curve [-]
$m_l$	Line bending moment [Nm/mm]
$r$	Root width [mm]
$T_\sigma$	Scatter range index
$\delta_b$	Degree of bending [-]
$\epsilon_{n,FEM}$	Nominal strain read from FE model [ $\mu\text{m}/\text{m}$ ]
$\epsilon_{n,SG}$	Measured nominal strain [ $\mu\text{m}/\text{m}$ ]
$\sigma_{n,w,loc}$	Local nominal weld stress [MPa]
$\sigma_w$	Weld nominal stress [MPa]
$\sigma_{ws}$	Structural weld stress in leg section [MPa]
$\sigma_{wm}$	Weld membrane stress in leg section [MPa]
$\sigma_{wb}$	Weld bending stress in leg section [MPa]

**Table 1**

Definitions of different stress-based approaches for weld root fatigue analysis [4,5].

Stress-based approach	FAT class	Stress analysis approach
Nominal weld stress	36, 40, or 45 according to joint type	Beam theory
Local nominal weld stress	36 or 40 according to joint type	Coarse FE model for defining local weld force to calculate nominal stress at weld throat
Structural weld stress	80	Coarse FE model for defining local weld force and secondary moment to calculate structural stress at weld root
Effective notch stress	225	Fine mesh FE-model with weld root modelled with a 1-mm radius. First principal stress read at root.

with partial penetration welds or fillet welds.

The influence of secondary bending stress in the weld is not considered in the nominal weld stress approach or local nominal weld stress approaches since they consider only the weld force component normal to the weld and the area of the weld cross-section; see Eq. (1). The simplest approach to also include the bending moment component is the structural weld stress approach. Sorensen et al. [10] used a fine-mesh FE-model extrapolating the principal stress, read in the 45° plane, through two points to the weld root. Alternatively, Fricke [11] used the weld force and bending moment components read from the weld leg plane, calculating the stress with beam theory by using these two load components and the weld leg length. In this approach, the weld

leg plane is used for calculating the stress since the fatigue crack path was found to be closer to it compared to the 45° plane. In the IIV recommendation, a FAT71 curve is given for stresses calculated at the throat section [5] whereas FAT80 is used for stresses calculated at the weld leg section [4].

To consider the effect of the weld root stress concentration on the modelling, several more refined local approaches have been introduced; see e.g. [12–15]. The most common local approach with a very fine mesh is the effective notch stress (ENS) approach. Considering the stress concentration at the weld root, it is obviously more accurate than the nominal or structural stress approaches, but also requires the greatest analysis effort. In this approach FE modelling is required, noting that for 2D cases, ENS stress concentration factors are also available in the literature [16]. The FE model geometry needs to include the weld geometry with a 1-mm radius modelled to the root and toe lines with a requirement of a mesh size of ¼ of the radius when higher-order elements are used. The 1-mm radius is valid for plate thicknesses  $t \geq 5$  mm, whereas a smaller radius is recommended for smaller plate thicknesses [17]. On the weld root side the 1-mm radius circle is positioned to touch the actual root line, i.e. to prevent reduction of the modelled throat

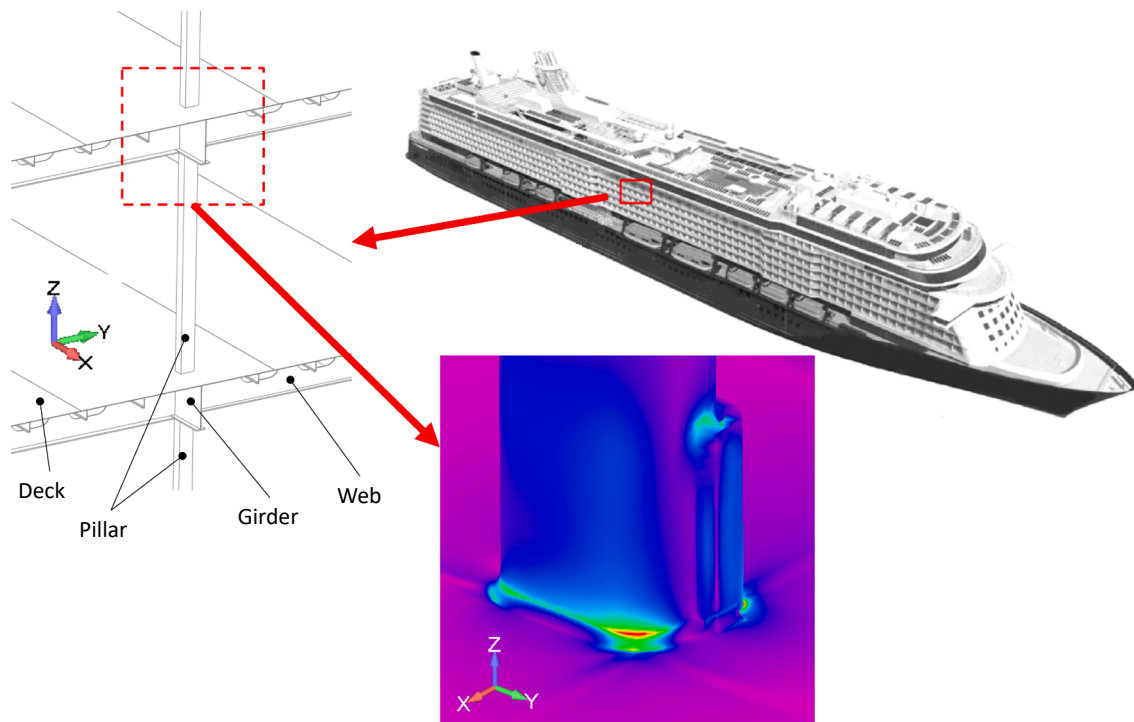


**Fig. 1.** Stress concentration of complex RHS pillar connection in continuous pillar line.

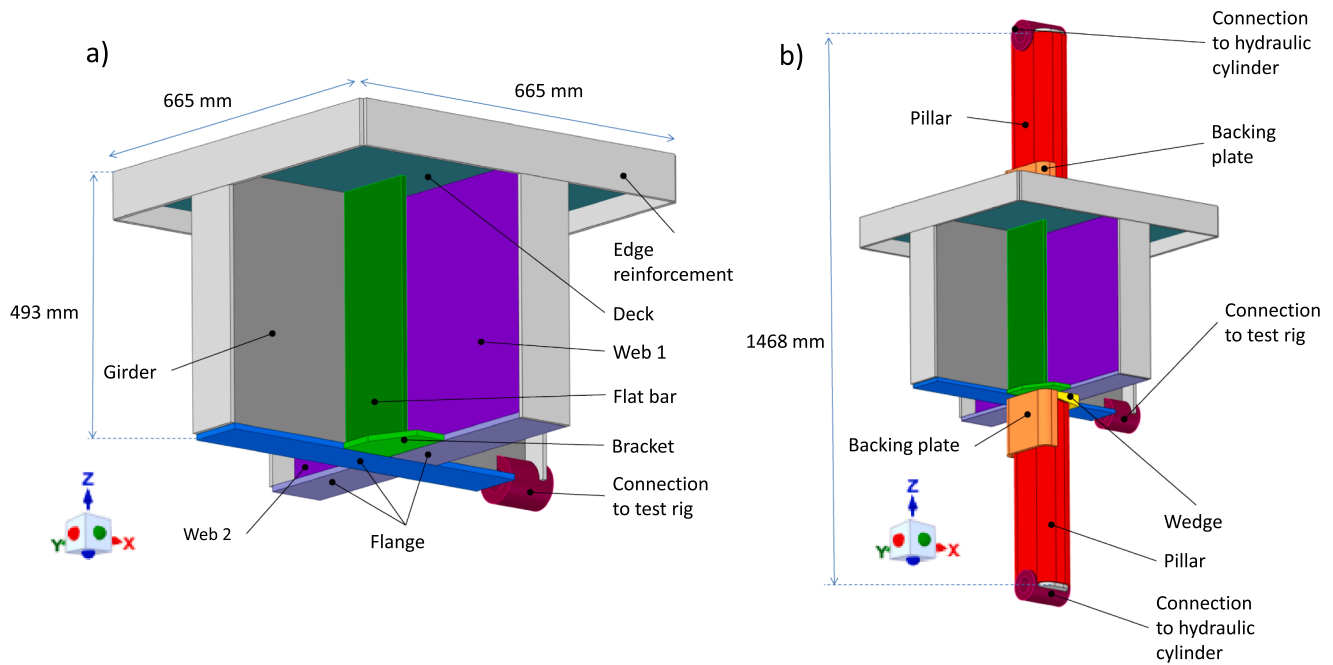


Fig. 2. Test specimen components of girder intersection structure (a) and full-scale specimen assembly (b).

Table 2  
Test specimen profiles and material properties.

	Deck	Flat bar	Girder	Web	Flange	Backing plate	Wedge	Bracket	Pillar
Thickness/ profile [mm]	5	10x150	7	7	10x100	10	150x90x35	10	RHS 150x100x12.5
Material *	NV A	VL A	NV A	NV A	VL A	S355MC	S355K2 + N	NV A	S355J2H
R <sub>y</sub> [MPa]**	321	322	330	330	288	419	343	302	549
R <sub>u</sub> [MPa]**	434	417	430	430	422	521	534	436	624
A%**	35	34	34	34	36	31	29	35	20.24
R <sub>y</sub> [MPa]***	235	235	235	235	235	355	355	235	355
R <sub>u</sub> [MPa]***	400–520	400–520	400–520	400–520	400–520	430–550	470–630	400–520	510–680
A%***	22	22	22	22	22	23	20	22	20

\* NV A is a DNV certified steel grade and VL A is a DNV GL certified steel grade with a minimum yield strength of 235 MPa.

\*\* Typical value from material specification

\*\*\* Nominal value

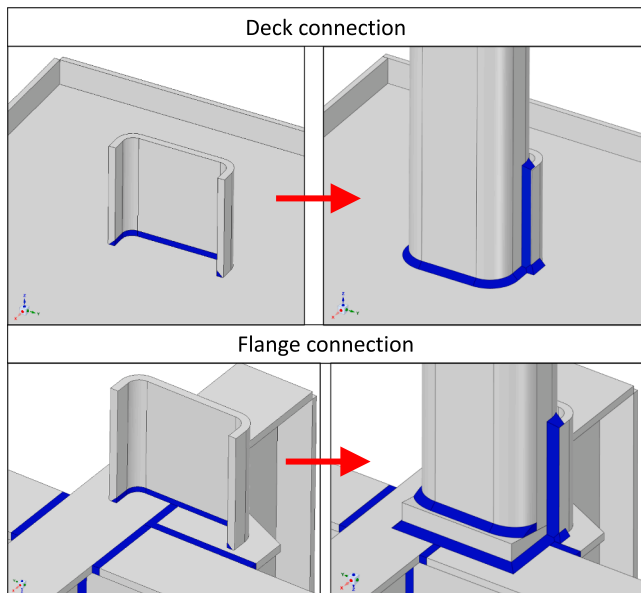


Fig. 3. Deck and flange connection welding arrangement.

thickness. The first principal stress is used as the reference stress read at the surface of the radius. For  $t \geq 5$  mm, the FAT225 class is used, regardless of the weld and joint type. Because of the small element size, a sub-modelling technique is often required. A drawback of this approach is that the approach is sensitive to the local modelling technique that is applied [18,19]. Moreover, as the fatigue test data is typically presented for small-scale specimens with 2D cross-sections or simplified 3D specimens [20], the validity of the approach for a complex 3D connection containing severe weld force concentrations along the weld seam remains unclear. In the case of a complex 3D connection, the basic assumption of ENS that the local stress at the location of fatigue crack initiation can be used to predict the fatigue strength of the whole connection can be violated.

To find the most suitable engineering approach for the fatigue design of complex connections in large structures, further investigations are needed. From the FE analysis perspective, the local nominal weld stress and structural weld stress approaches are attractive choices as they do not require time-consuming fine-mesh FE modelling. A low-effort approach called the traction force approach was recently introduced by Rautiainen et al. [8] to capture local weld loads for use in the LWNS approach. However, it is not clear what the proper FAT class for complex welded connections is. This is because in the standards the FAT class is given for simplified 2D structures. On the other hand, the ENS approach is an attractive choice because of its clear way of determining stress, but

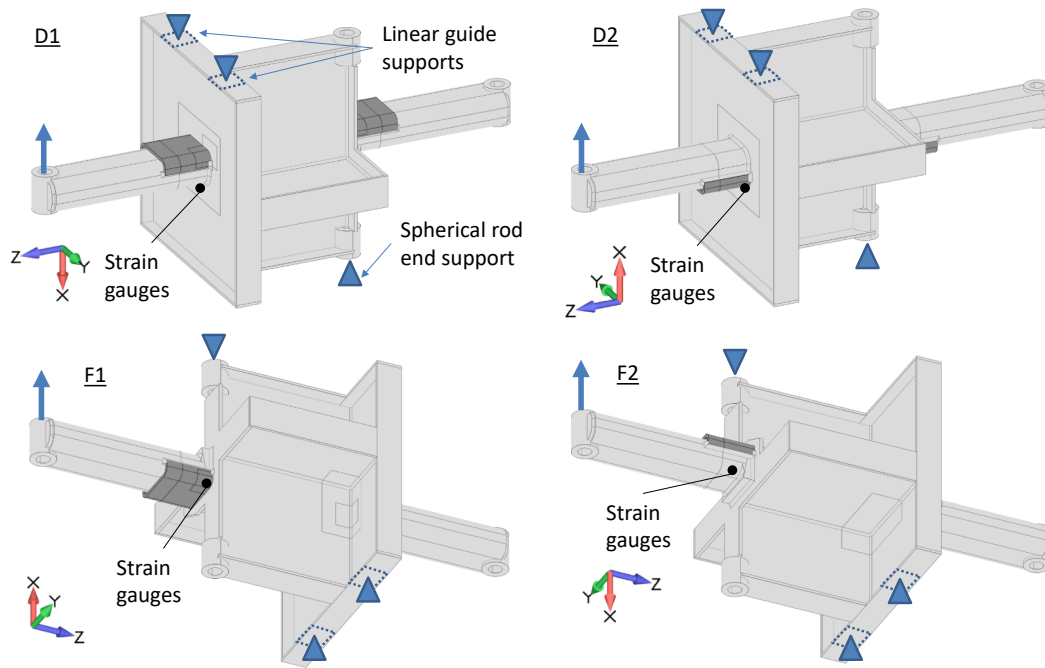


Fig. 4. Test setups where X-axis deformation is suppressed with linear guides and pinned boundary condition created with a spherical rod end.

Table 3  
Naming of fatigue tests according to test specimen and test setup.

Test specimen	S01	S02	S03	S04	S05	S06	S07	S08
Deck connection tests	S01-D1	S02-D1	S03-D1	S04-D1	S05-D1	NaN	S07-D1	S08-D2
Flange connection tests	S01-F1	S02-F1	S03-F1	S04-F1	S05-F1	S06-F1	S07-F1	S08-F2

requires, however, time-consuming FE-modelling. For ENS it is also not clear if FAT225 is valid regardless of the weld type or complexity of the connection. Therefore, more research is needed to investigate the validity of these approaches for complex connections with severe force concentrations along the weld seam. To study the fatigue strength of complex connections, full-scale tests are needed. Full-scale fatigue tests have been performed to investigate weld toe failure [1,3,21] but very little test data can be found for weld root failure in load carrying cruciform connections and mainly simplified structures have been tested [9,11,20].

In this paper fatigue tests are presented for complex full-scale specimens representing the pillar connection of a cruise ship. Altogether 15 fatigue tests were carried out for structures including fillet welds, partial penetration welds, and partially penetrated fillet welds. The full-scale test specimens have RHS pillars welded onto a section of the web-to-girder intersection, which is typical in ship structures. The test specimens are loaded by three-point cantilever bending load. The fatigue analysis is carried out with the LWNS, structural weld stress and ENS approaches. The FE models created for the test specimens are based on detailed geometry measurements, thereby including scantling misalignment as well as weld cross-section dimensions. Finally, the FE models are compared with the measured strains and a comparison of the predicted and actual fatigue life as well as failure modes, is presented.

## 2. Method

### 2.1. Test specimen

The structure and components of the test specimen are described in Fig. 2 and in Table 2. The girder intersection structure is a typical structure in cruise ships, where longitudinal and transversal deck girders intersect. Pillars are used in cruise ships to provide the required vertical stiffness to the hull. Eight full-scale test specimens (entitled S01...S08) were produced at the Meyer Turku shipyard using conventional ship-building steel grades. The test specimen, representing a repeating unit of the continuous pillar line on a cruise ship superstructure and shown in Fig. 1, consists of RHS pillars welded onto the girder intersection structure using connector parts between the pillar and girder intersection. The specimens were designed to have two different connections with varying fatigue critical weld types, i.e. single-sided partially penetrated fillet welds (SSPPFW), double fillet welds (DFW), and partial penetration welds (PP). Each of these two connections was tested separately, one representing the deck and the other the flange connection under bending loading similar to ship hull deformations. The weld dimensions for both connections were selected to be such that fatigue failure would be at the root side. The S06 deck connection test specimen was tested for weld toe fatigue with a different scantling arrangement and therefore it was left out from the present paper.

As shown in Fig. 2, the girder intersection structure between the pillars consists of intersecting T-profiles (Webs, Girder and Flange) and a deck plate, reinforced with a flat bar and a bracket. To prevent the edges of the webs, girder, and deck plates from deforming, they are reinforced with flat bars at the edge. Finally, the structure is equipped with a threaded stud as a connection to the test rig. On the deck and flange, RHS profiles are welded using a C-shaped backing plate needed for the pillar assembly. In actual structures such as in cruise ships, the backing plate is used if the rear side of the connection is not accessible for welding because of the surrounding outfitting. On the flange connection in addition to the backing plate, a wedge is also used between the RHS and the flange. In actual structures, a wedge is used when the pillar cannot be directly welded to the flange when the distance between the deck and flange varies because of manufacturing tolerances. The end of the RHS profile is equipped with a threaded stud to be connected to the

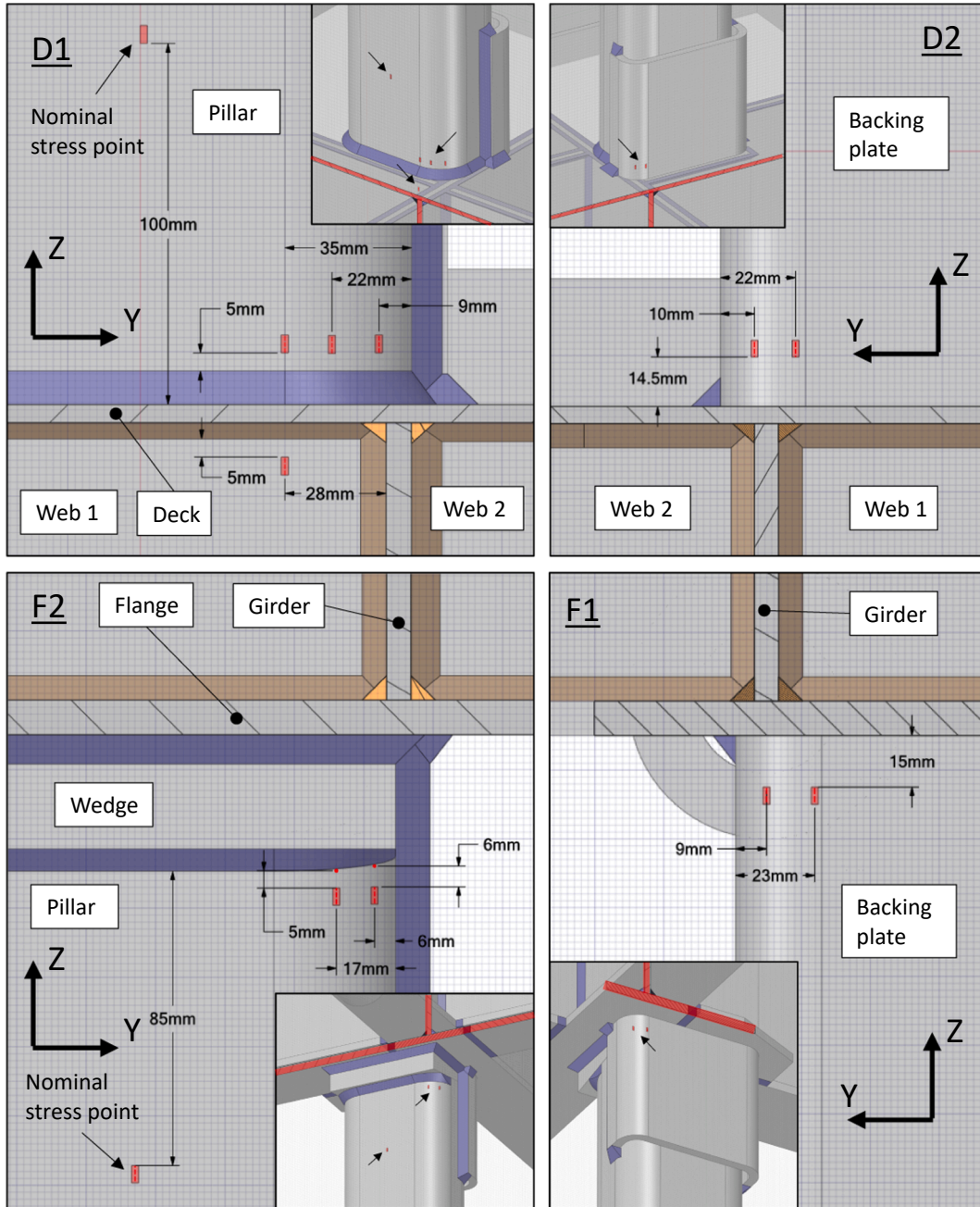


Fig. 5. Strain gauge locations. For the test setups D1 and F2 the section cut plane is in front of pillar. For the test setups D2 and F1 the section cut plane is behind the backing plate.

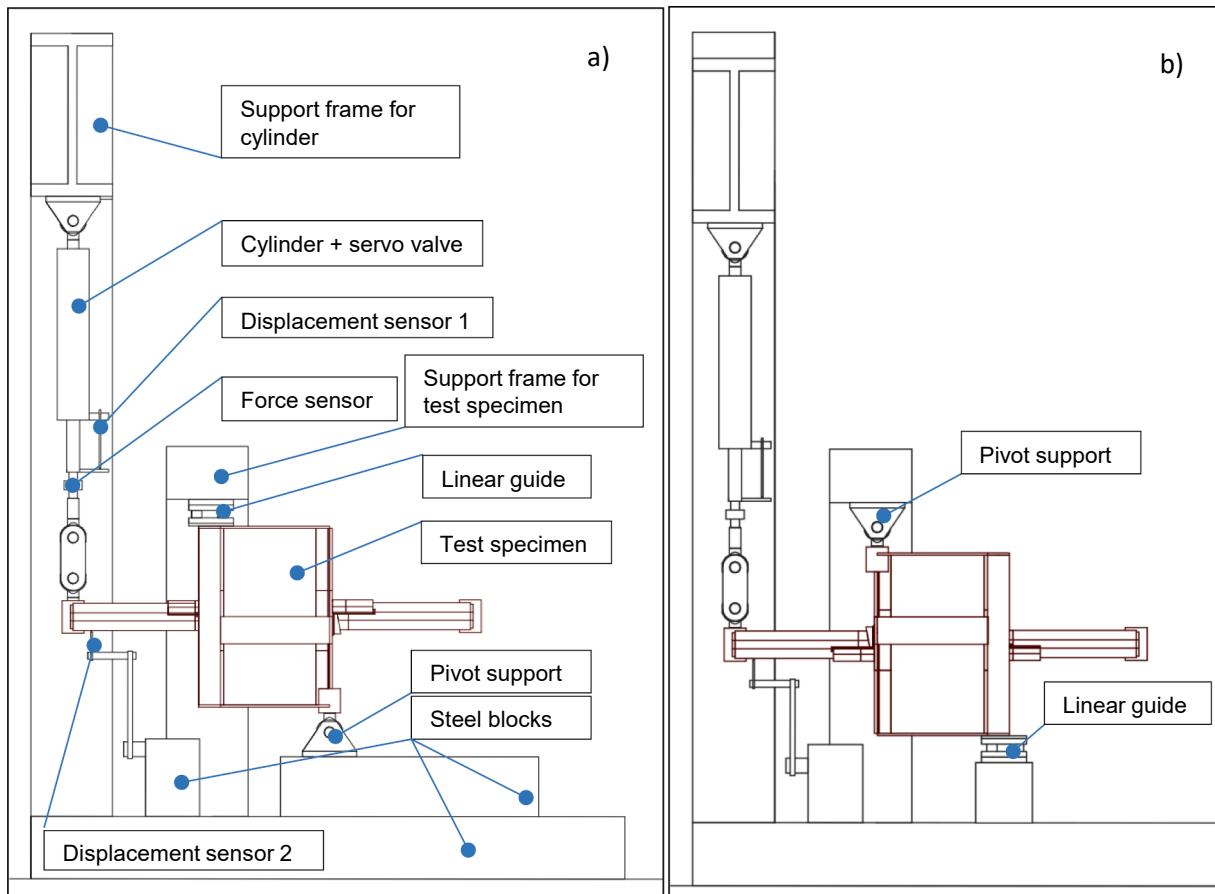


Fig. 6. Test setup for deck connection test D1 (a) and flange connection test F1 (b).

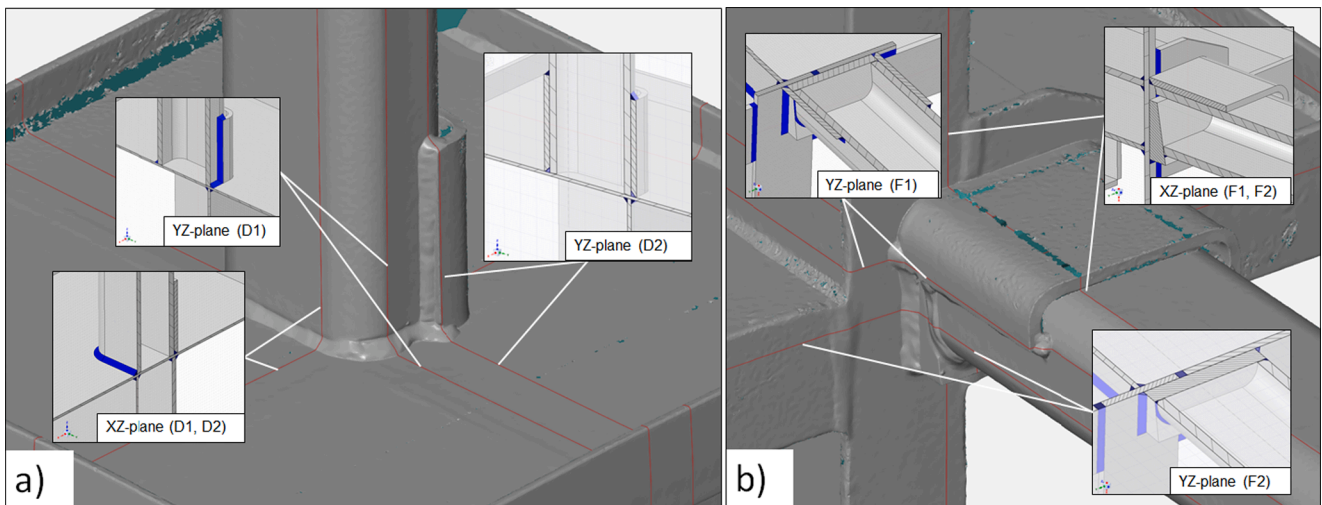


Fig. 7. Planes for measuring misalignment in deck connection test setups D1 and D2 (a) and flange connection test setups F1 and F2 (b).

hydraulic cylinder using a spherical rod end. Apart from the butt welds between the flanges and bracket, all the welds in the girder intersection structure are double fillet welds (DFW). Manual MAG welding was used with Filarc 6113 d1.2 mm welding wire.

Fig. 3 shows the welding arrangement of the RHS pillar at the connection of the deck and flange. In both connections first the C-shaped backing plate is welded with a partial penetration weld (PP) from inside the profile, leaving the weld root side on the outer surface of the backing plate. The depth of the weld groove is 8 mm. For the deck side

connection, in the second phase, the RHS profile is fitted onto the backing plate and welded to the deck with a single-sided partially penetrated fillet weld (SSPPFW). The vertical edges of the backing plate are welded with fillet welds (FW). For the flange connection, in the second phase the RHS profile is fitted onto the backing plate and a wedge is fitted between the RHS profile and the flange. The distance between the surfaces of the RHS and the wedge is set to 15 mm. The RHS pillar is welded to the wedge with an SSPPFW weld and the wedge welded to the flange with fillet welds (FW). The vertical edges of the

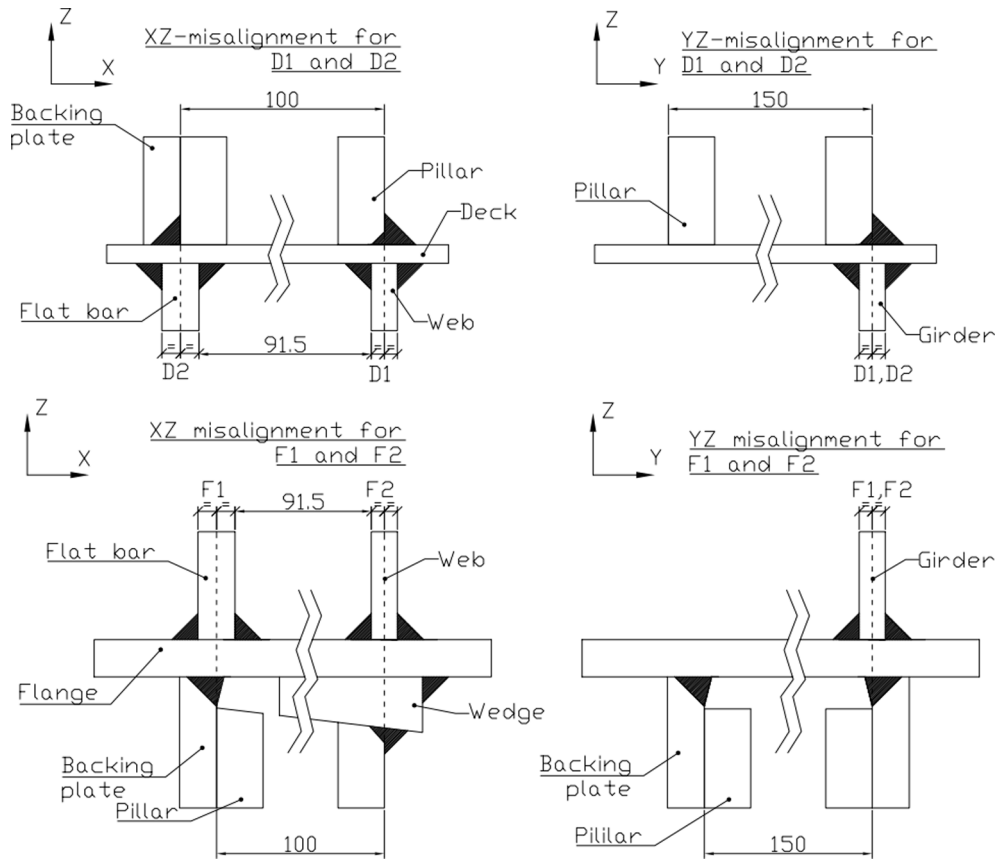


Fig. 8. Zero misalignment arrangement and coordinate system for the defining sign of the misalignment.

Table 4

Measured misalignment values [mm], deck connection.

Test specimen ID	S01-D1	S02-D1	S03-D1	S04-D1	S05-D1	S06	S07-D1	S08-D2
XZ-plane eccentricity	1.1	1.0	0.7	-3.4	-4.4	NaN	-0.7	-3.4
YZ-plane eccentricity	3.3	4.4	3.7	-1.8	-4.1	NaN	-0.3	0.0

Table 5

Measured misalignment values [mm], flange connection.

Test specimen ID	S01-F1	S02-F1	S03-F1	S04-F1	S05-F1	S06-F1	S07-F1	S08-F2
XZ-plane eccentricity	2.5	0.8	1.1	-6.2	-5.2	-0.1	1.5	0.2
YZ-plane eccentricity	-0.6	-2.8	3.6	-7.7	-4.9	0.5	-9.2	-8.3

backing plate are welded with fillet welds (FW). As for both connections, at both ends of the edge of the backing plate short fillet welds (FW) are added along the X-axis. For both connections, the RHS groove depth for a partial penetration weld is 4.5 mm.

### 2.2. Test setup

Fatigue tests were carried out using three-point bending loading. This loading arrangement represents the actual pillar shear loading with sufficient accuracy. This loading condition is created when the ship superstructure deforms under wave-induced bending, causing relative movement between the decks. For each specimen two tests were carried out to test both the deck and the flange connection. Moreover, one specimen (S08) was loaded in the opposite direction by rotating the test specimen through 180° about the pillar axis. Therefore, in total four loading conditions (D1, D2, F1, and F2) were created, as shown in Fig. 4, with the naming of each test according to the test setup given in Table 3.

As shown in Fig. 4, X-axis deformation of the flat bar at the edge was suppressed by using linear guides and a pinned boundary condition was created with a spherical rod end. 5-mm grid strain gauges were installed on the test specimens to validate the simulations in terms of the nominal stress and local stress at fatigue critical locations. The location of the strain gauges is shown in Fig. 4 and in more detail in Fig. 5.

The detailed arrangement for the test setups D1 and F1 is shown in Fig. 6. The test specimen was supported at three points: two support points with linear guides on the flat bar at the edge, and a spherical rod end connected to a threaded stud (see also Fig. 4). The linear guides were positioned on both sides of the girder plate. The connection between the linear guides and flat bar was arranged in such a way that the flat bar could deform in the YZ-plane. The load was applied at the end of the pillar using plates to allow free rotation between the test specimen and hydraulic cylinder. A load ratio  $R = 0.1$  and a frequency of 2 Hz were used in the fatigue test.

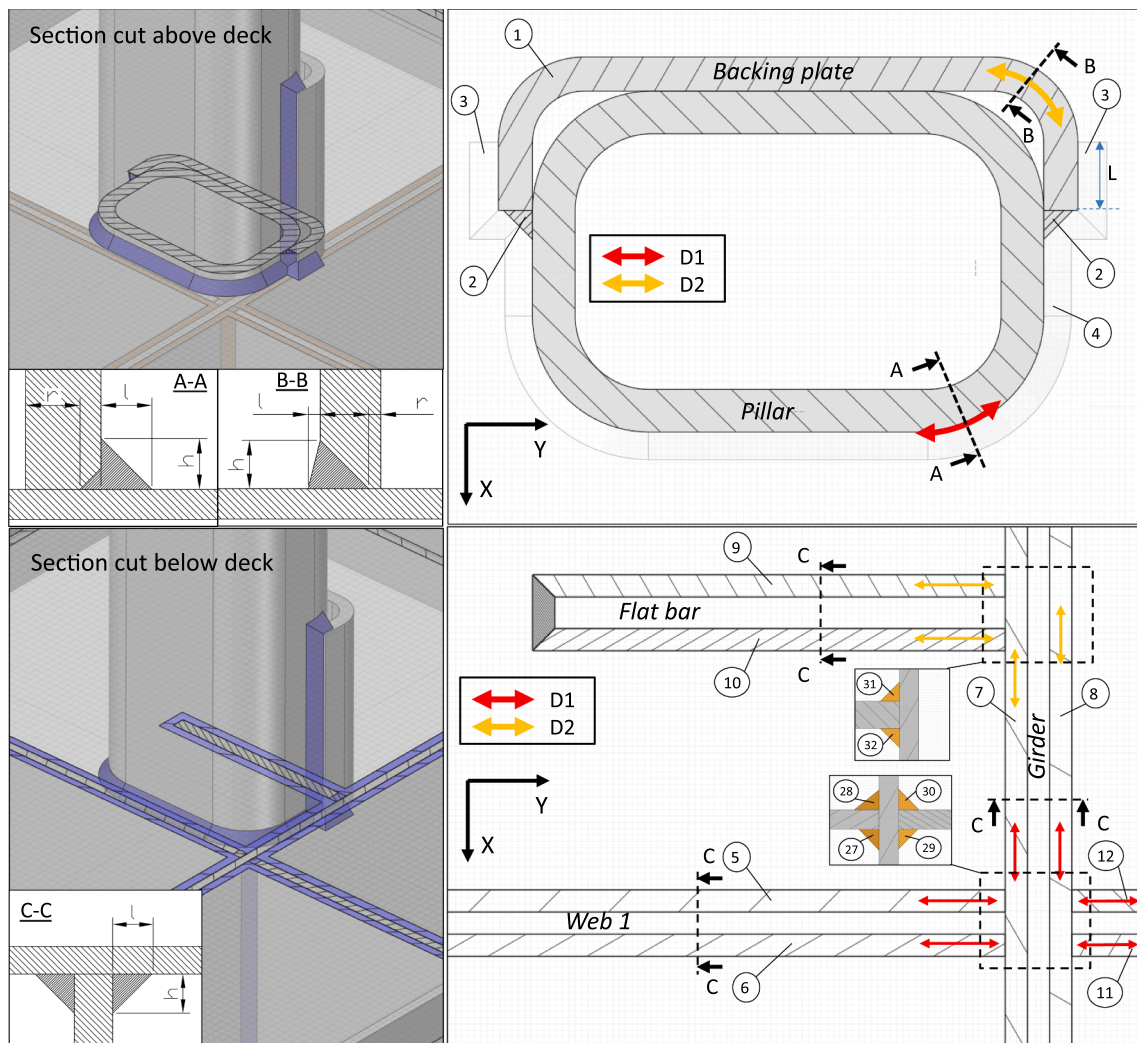


Fig. 9. Measured critical welds, deck connection.

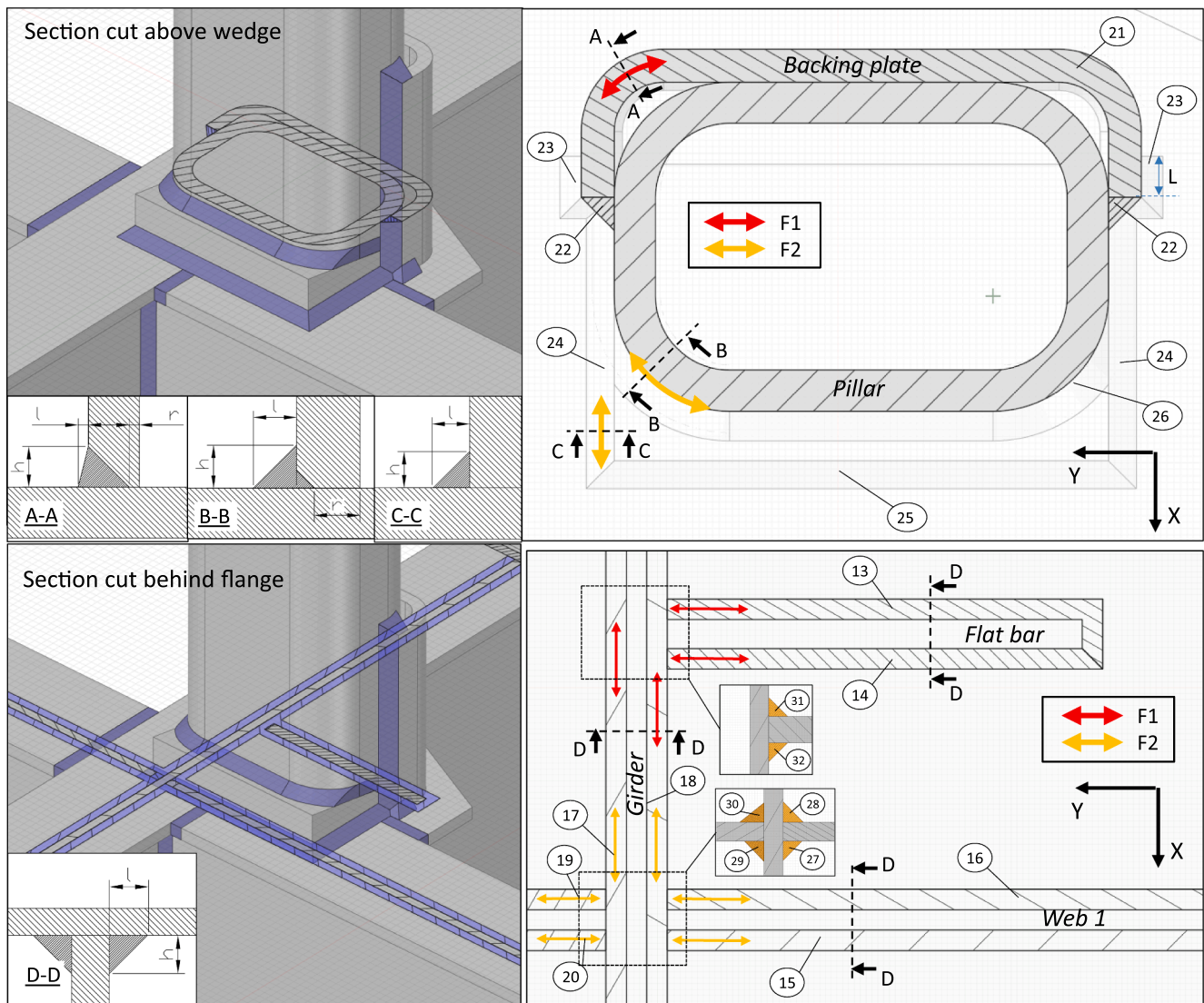


Fig. 10. Measured critical welds, flange connection.

**Table 6**

Weld cross-section dimensions [mm]. Values are given in the following order:  $r | h | l$  with  $r$  given only for welds nos. 1, 4, 21, 23 and 26. For welds nos. 3 and 23 values are given in the following order:  $L | h | l$ . An equilateral fillet weld throat thickness, e.g. a5 representing a typical weld size, is reported for welds under compressive loading.

	Plate 1	Plate 2	Weld type	S01	S02	S03	S04	S05	S06	S07	S08
1	Backing plate	Deck	PP	0   0   0	0   0   0	0   0   0	0   0   0	0   0   0	–	0   0   0	2.5   9   2
2	Backing plate	RHS	FW	a6	a6	a6	a6	a6	–	a6	a6
3	Backing plate	Deck	FW	20 8.5   8.5	20 8.5   8.5	20 8.5   8.5	20 8.5   8.5	20 8.5   8.5	–	20 8.5   8.5	23 9.2 8.3
4	RHS	Deck	SSPPFW	7.5 9.3 6.9	9.5 8.4 8.6	9.4 8.4 8.6	12.2  8.2 8.1	7.5 8.2 8.3	–	9.3 7.9 7.2	10.0 9.0 8.5
5	Web 1 in	Deck	DFW	4.7 6.0	4.5 7.5	6.1 6.0	6.5 7.5	5.0 6.1	–	6.0 5.9	a5
6	Web 1 out	Deck	DFW	4.5 5.7	4.3 6.7	5.7 6.5	6.0 5.7	5.7 6.8	–	5.8 5.3	a5
7	Girder in	Deck	DFW	5.5 7.1	4.6 4.6	4.9 6.5	6.5 6.3	5.9 6.9	–	6.5 6.1	4.6 6.2
8	Girder out	Deck	DFW	5.7 6.4	4.4 6.6	4.9 6.0	5.0 5.3	5.3 6.0	–	5.7 6.4	4.5 5.5
9	FB out	Deck	DFW	a5	a5	a5	a5	a5	–	a5	6.3 8.0
10	FB in	Deck	DFW	a5	a5	a5	a5	a5	–	a5	7.7 7.7
11	Web 2 out	Deck	DFW	5.2 6.3	4.5 6.3	3.7 5.6	5.2 5.2	6.3 6.8	–	5.7 6.4	a5
12	Web 2 in	Deck	DFW	7.1 7.1	3.9 6.7	5.6 6.1	5.2 7.1	5.1 7.5	–	6.5 6.1	a5
13	FB out	Flange	DFW	7.5 7.3	7.1 7.7	9.5 9.1	7.5 7.7	6.9 6.7	6.8 8.5	8.0 7.3	a5
14	FB in	Flange	DFW	8.9 10.7	9.3 10.9	7.7 7.6	8.2 8.2	7.7 6.9	7.8 8.1	8.5 7.1	a5
15	Web 1 out	Flange	DFW	a5	a5	a5	a5	a5	–	a5	6.0 6.2
16	Web 1 in	Flange	DFW	a5	a5	a5	a5	a5	–	a5	6.7 5.0
17	Girder out	Flange	DFW	4.9 5.6	7.1 6.4	5.1 5.7	4.6 4.8	5.6 5.6	4.5 5.6	5.2 5.5	4.3 5.3
18	Girder in	Flange	DFW	5.4 5.9	7.1 4.9	5.6 4.2	4.9 6.9	6.8 6.9	4.3 5.8	5.6 5.6	4.4 6.3
19	Web 2 in	Flange	DFW	a5	a5	a5	a5	a5	–	a5	6.8 6.2
20	Web 2 out	Flange	DFW	a5	a5	a5	a5	a5	–	a5	6.2 6.7
21	Backing plate	Flange	PP	1.5 9 2.5	4 9 2.5	2.5 10 1	1.4 9 1.5	3 9 3.5	3 9 3	2 10 3	0   0   0
22	Backing plate	RHS and wedge	FW	a7.1	a7.1	a7.1	a7.1	a7.1	–	a7.1	a7.1
23	Backing plate	Flange	FW	12.5 8.3 6.5	10 9.1 7.7	12 7.6 5.7	18 7.8 7.3	15 7.9 5.2	13 8.2 5.1	24 8.3 7.2	46.2 8.3 6.7
24	Wedge	Flange	FW	a6	a6	a6	a6	a6	–	a6	9.2 7.0
25	Wedge	Flange	FW	a6	a6	a6	a6	a6	–	a6	10.6 9.5
26	RHS	Wedge	SSPPFW	9.1 9.1  12.7	9.1 9.1  12.7	9.1 9.1  12.7	9.1 9.1  12.7	9.1 9.1  12.7	9.1 9.1  12.7	9.1 9.1  12.7	9.1 9.1  11.9 9.3 13.4
27	Web 1 out	Girder - Deck	DFW	7.1 7.4	7.2 7.2	7.2 7.5	6.4 6.4	8.3 8.8	–	8.0 8.3	a5
	Web 1 out	Girder - Flange	DFW	a5	a5	a5	a5	a5	–	a5	9.6 7.1
28	Web 1 in	Girder - Deck	DFW	8.3 6.9	7.7 7.2	9.0 7.2	8.6 7.9	8.4 7.6	–	7.9 6.3	a5
	Web 1 in	Girder - Flange	DFW	a5	a5	a5	a5	a5	–	a5	7.3 5.8
29	Web 2 out	Girder - Deck	DFW	8.4 7.0	6.9 5.7	6.9 7.1	6.7 7.2	9.0 8.3	–	7.8 7.9	a5
	Web 2 out	Girder - Flange	DFW	a5	a5	a5	a5	a5	–	a5	8.1 8.2
30	Web 2 in	Girder - Deck	DFW	6.8 6.3	7.8 7.7	7.4 7.5	8.6 9.2	7.0 7.4	–	7.8 7.9	a5
	Web 2 in	Girder - Flange	DFW	a5	a5	a5	a5	a5	–	a5	6.8 8.4
31	FB out	Girder - Deck	DFW	a5	a5	a5	a5	a5	–	a5	9.4 9.2
	FB out	Girder - Flange	DFW	7.4 5.6	7.7 8.1	10.2 7.2	8.6 6.5	8.2 7.9	8.7 8.5	9.5 9.4	a5
32	FB in	Girder - Deck	DFW	a5	a5	a5	a5	a5	–	a5	8.0 9.1
	FB in	Girder - Flange	DFW	8.9 10.2	6.7 7.8	8.6 8.1	9.6 8.4	7.2 10.3	8.0 10.1	6.4 7.1	a5

2.3. Geometry measurements

Optical scanning for all the test specimens was carried out using GOM Atos [22]. The accuracy of the measurements was 0.02 mm. The GOM Inspect software was used to measure eccentricity and the Space Claim software [23] to measure the weld profiles.

2.3.1. Misalignment

The scantling misalignment, i.e. the eccentricity between the welded plates, was defined from the planes in the fatigue critical areas shown in Fig. 7. Zero misalignment in the XZ-plane is considered when the outer surface of the RHS is aligned with the mid-surface of the underlying web in the test setups D1 and F2 or with the mid-surface of the flat bar in the test setups D2 and F1 (see also Fig. 4). Zero misalignment in the YZ-plane is considered when the outer surface of the RHS is aligned with the mid-surface of the underlying girder as shown in Fig. 8.

In each test setup, positive misalignment is considered when the pillar, the backing plate, and the wedge are moved along the positive X- or Y-axis according to the coordinate system in Fig. 8, maintaining the girder intersection structure in place. The misalignment values are shown in Table 4 and Table 5. The average distance between the inner surfaces of the web and the flat bar is 91.5 mm.

2.3.2. Weld cross-section dimensions

The measured weld cross-section dimensions were utilised in FE modelling in the fatigue critical area and to define the correct throat thickness  $a_w$  for calculating the local nominal weld stress. Since fatigue critical welds are under tensile loading, every individual weld in tension was measured distinctly, while a typical weld size was used for all the welds on the compressive side. All the individual welds were designated with a number (1...32) shown in Fig. 9 and Fig. 10 for the deck and flange connections respectively, and the results are presented in Table 6. The welds nos. 27...32 are further separated into the region close to the deck and the region close to flange, as reported in Table 6. The weld profile is defined with the weld leg height  $h$  and leg length  $l$  for the fillet welds and also the root depth  $r$  for the partial penetration welds.<sup>1</sup> For the fillet welds nos. 3 and 23 on the side of the backing plate, weld length  $L$  is also given. In Table 6 the values are given in the following order:  $r | h | l$  with  $r$  given only for welds no. 1, 4, 21, 23 and 26. For welds no. 3 and 23 values are given in following order:  $L | h | l$ . For welds under compressive loading, typical dimensions are given that assume an equilateral fillet weld. In these cases only the fillet weld throat thickness is reported, e.g. a5.

Because of manual welding, some fluctuation in the weld throat

<sup>1</sup> The root depth was measured from the fracture surface after the tests.

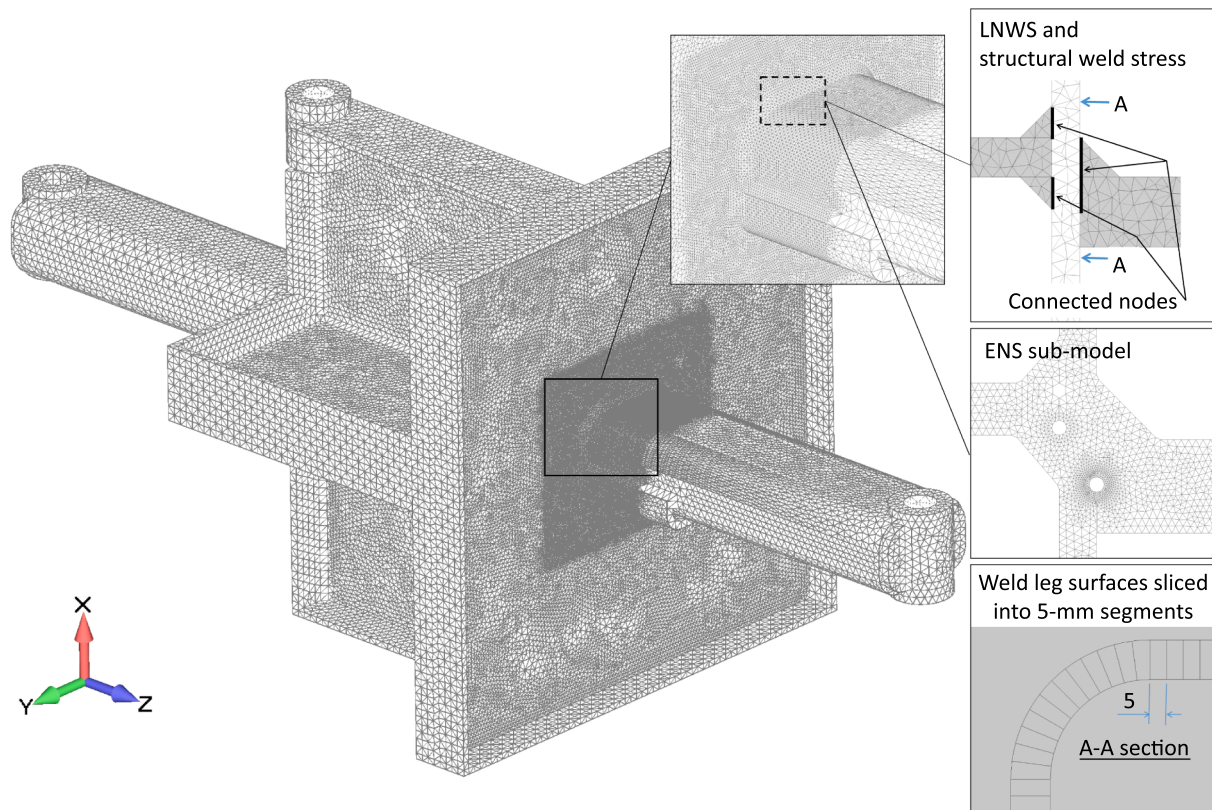


Fig. 11. Test specimen FE model.

thickness along the welds was observed. Since the weld profile in the fatigue critical area is considered to have the greatest influence on local stiffness and thereby on the distribution of loads to individual welds, measurements were taken distinctly from the area of the peak weld forces predicted by the Finite Element Method.<sup>2</sup> In Fig. 9 and Fig. 10 the red arrows show the measurements for the specimens S01...S07 (test setups D1 and F1) and the orange arrows those for the specimen S08 (test setups D2 and F2).

#### 2.4. FE analysis

From each test specimen an FE model is created with FEMAP [24] and NX Nastran [25] using 10-noded solid parabolic tetrahedron elements (CTETRA). First, global models were created with the objective being to define the local nominal and structural weld stresses. In the global model, the welded joints were modelled with a continuous mesh, leaving the root faces unconnected, as shown in Fig. 11, and without any contacts. Second, sub-models were created for the effective notch stresses (ENS). Rigid elements were modelled and connected to the inner surface of the threaded stud to apply load and boundary conditions. Linear guides were modelled by fixing X-axis translation on the surface of the flat bar within the area shown in Fig. 4. To identify the local weld forces and secondary bending moments, the weld leg surfaces were

sliced into 5-mm-long segments. For the global model, an element size of 2.5 mm was used within the connection region and a 10-mm element size elsewhere. ENS analyses with a 1-mm radius were created according to the instructions by Fricke [4] using 3D sub-models from critical areas with a typical model size of 100x100x100 mm. An element size of 0.25 mm was used around the weld radius. In the vicinity of the refined areas, an element size of 1 mm was used and closer to the edges of the model an element size of 2.5 mm was used.

### 3. Results

#### 3.1. Primary fatigue failure location

During the fatigue tests crack initiation and propagation were observed visually. All the cracking sites are numbered in Fig. 12, which also show an example photo of a detected crack. The observations are reported in Table 7, which gives the crack site, crack length, and number of cycles. In many tests multiple crack locations were observed since the cracking of the weld root is visible only when it has growth through the weld. In such cases the primary failure location was concluded to be the longest cracked weld.

#### 3.2. Number of cycles to local cracking

As can be seen in Table 7, in many cases the first observed crack was already propagated far, e.g. to half of the pillar width. To estimate the number of cycles to local cracking  $N_{loc}$ , the reduction in the strain range at the critical location was utilised from the test specimen S01-D1, where the first detected crack was short, i.e. 20 mm. The corresponding strain

<sup>2</sup> The measurements were taken as a typical value over a distance of about 20 mm across the point of peak tensile weld force. If the peak weld force existed at a weld intersection that was not visible for measurements, the measurement was taken next to the weld intersection area. For vertical welds of the web, girder, and flat bar, the measurement was taken as a typical value within about 20 mm from the intersection point downwards. Depending on the test setup, i.e. the side of the tensile loaded region, the measurements were taken from two different locations.

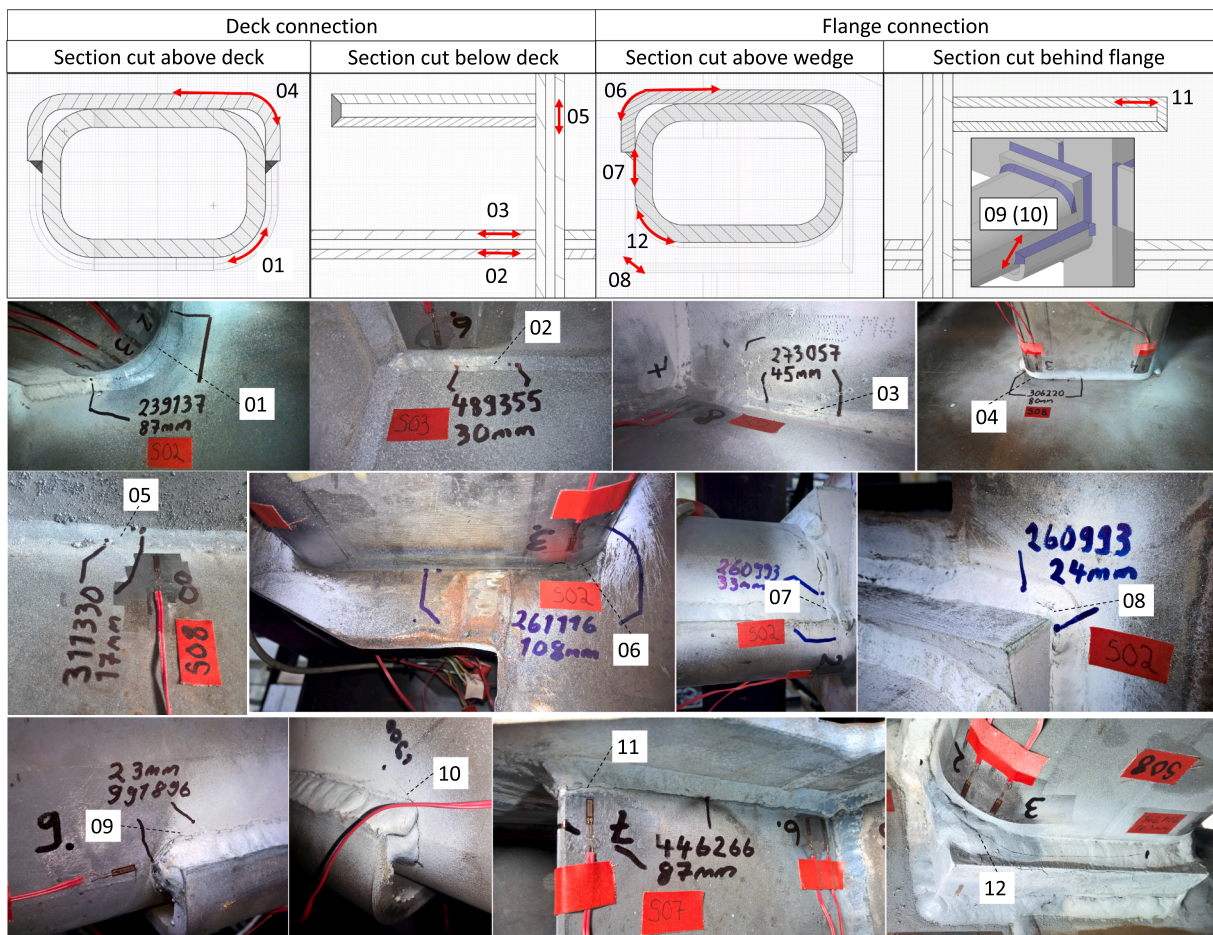


Fig. 12. Fatigue crack sites and examples of detected cracks.

**Table 7**

Fatigue crack observations given the crack site, crack length [mm], and number of cycles. Subscript *t* stands for weld toe cracking.

Test specimen	Test setup	Detected crack site   length [mm]   number of cycles					Primary fatigue failure site
		1	2	3	4	5	
S01	D1	01 20  389 773	02 55  398 602	02 87  446 200	01 47  447 100	03 88  456 720	02
S02	D1	01 87  239 137	02 12  250 990	02 36  256 164	01 97  258 110	01 125  259 892	01
S03	D1	01 48  489 355	02 30  489 355	02 49  503 985	01 61  526 490	02 75  534 561	01
S04	D1	02 57  2 017 083	03 41  2 017 083	03 60  2 219 354	02 82  2 219 354	01  39  2 219 354	02, 03
S05	D1	01 51  1 108 161	01 65  1 153 769	01 108  1 308 709	01 143  1 448 235	01 155  1 467 769	01
S07	D1	01 129  271 582	01 172  281 982	01 210  299 239	–	–	01
S08	D2	04 80  306 220	05 17  311 330	04 105  328 730	–	–	04
S01	F1	07 40  770 000	06 126  779 570	09  16  780 216	11  63  780 900	07 18  780 986	06
S02	F1	08 24  260 993	07 33  260 993	06 108  261 116	06 159  268 015	09  15  268 015	06
S03	F1	06 70  1 407 749	06 177  1 610 565	–	–	–	06
S04	F1	09  23  991 896	10  40  1 900 000	09  44  1 900 000	09  49  2 200 975	10  43  2 200 975	06
S05	F1	08 ~18  1 328 000	06 55  1 339 564	09  37  1 340 325	08 37  1 340 795	07 12  1 394 414	06
S06	F1	07 ~25  471 000	06 70  487 296	07 ~36  486 731	09  29  486 957	08 33  500 379	06
S07	F1	06 187  446 266	11  87  446 266	09  23  446 266	–	–	06
S08	F2	12 163  366 706	12 187  380 675	12 227  381 712	–	–	12

range reduction of 55 % at the critical location was used to define the number of cycles to the local cracking of all the test specimens. In Fig. 13, the strain range decrease and connection stiffness reduction are shown for the two most common failure locations, i.e. the RHS-to-deck weld and backing plate-to-flange weld. The number of cycles to local cracking  $N_{loc}$  and the final number of cycles  $N_{final}$  are reported in Table A1.

3.3. Strain gauge measurements

The FE results are validated by comparing the strain measurement data with the strains from the FE model. The results are shown in Fig. 14 using 1-kN loading. In the text box, the measured strain  $\epsilon_{n,SG}$  and strain from FEM at the nominal stress  $\epsilon_{n,FEM}$  are shown. The strain measurements are in good agreement with the FE model, with the mean error being 8.9 % at the fatigue critical location and 2.3 % at the nominal stress location. This indicates that the force concentration in the FE model is captured with sufficient accuracy.

3.4. Local nominal weld stress analysis

The weld forces are taken from the weld leg surface of the primary failure location sliced into 5-mm-long segments as shown in Fig. 11 and divided by the weld throat thickness  $a_w$  according to Eq. (1). The nominal weld stress distributions are shown in Fig. 15. For S04-D1 a strong conclusion could not be drawn about the primary failure location between the crack sites O2 and O3. Therefore, in Fig. 15 the stress distributions of both of the welds are shown.

In Table 8 and Table 9 the local nominal weld stresses  $\sigma_{n,w,loc}$  and degree of bending  $\delta_b$

$$\delta_b = \frac{\sigma_{wb}}{\sigma_{wb} + \sigma_{wm}} \tag{2}$$

calculated at the weld leg section as in [11] are given for the most heavily loaded welds. Because in the test specimen S08 different welds are in tension, results are presented for different welds than for other specimens. The primary failure location is highlighted in green. In welds nos. 5, 13, and 14 the peak weld nominal stress was at the weld intersection in some specimens. In these cases, the degree of bending could not be defined and therefore is not reported.

The fatigue test results for local cracking with the LNWS approach are presented in Fig. 16, separating the failed welds according to weld type and to force concentration (FCF). The data points are given for an R = 0.1 load ratio and the calculated characteristic FAT class values for R = 0.5 by using a mean stress correction factor of 0.929 according to Sonsino [26] in order to compare them with the IIW recommendations. The result for the specimen S04-D1 is an average stress of welds no. 5

and 6 as a clear conclusion could not be drawn as to which one was the primary failure location. From Fig. 16 it can be seen that there is a clear difference between the fillet weld (SSPPFW and DFW) and partial penetration weld (PP), with the fatigue strength being higher for high FCF values of PP welds. This observation is highlighted in Fig. 16 with the two regions. A characteristic FAT class with a slope  $m = 3$  was FAT53 for fillet welds and FAT71 for partial penetration welds. The scatter range index was  $T_\sigma = 1.26$  for fillet welds and  $T_\sigma = 1.68$  for partial penetration welds. The results are compared with IIW FAT36, which corresponds to a fillet-welded cruciform connection with a ratio of the weld throat thickness  $a_w$  to the abutting plate thickness  $t$  over 1/3 [5]. The results are conservative with respect to the IIW fatigue class FAT36.

3.5. Structural weld stress and ENS analysis

The structural weld stress  $\sigma_{ws}$  as formulated in [8]

$$\sigma_{ws} = \sigma_{wm} + \sigma_{wb} = \frac{1}{L_w} \left( |f_i| + \frac{6|m_i|}{L_w} \right) \tag{3}$$

was calculated from the weld force  $f_i$  and bending moment  $m_i$ . As can be seen in Fig. 17a, the scatter range index  $T_\sigma$  (as described in [16]) is high i.e.  $T_\sigma = 4.98$ , and the characteristic curve is FAT44 i.e. below the IIW curve FAT80. The results are shown with respect to the degree of bending,  $\delta_b$  in the weld, showing that lower fatigue strength results in lower values of  $\delta_b$ . As can be seen from Fig. 17b, the scatter range index is also high for ENS i.e.  $T_\sigma = 5.40$  and the characteristic curve is FAT111 i.e. below the IIW curve FAT225. In the ENS results the stress concentration factor  $K_t$

$$K_t = \frac{ENS}{\sigma_{n,w,loc}} \tag{4}$$

is shown using colour coding, showing that lower fatigue strength results in a lower value of  $K_t$ . In both approaches, the stress was calculated at the primary failure location. The result for the specimen S04-D1 is the average stress of welds nos. 5 and 6 as a clear conclusion could not be drawn as to which one was the primary failure location. In Fig. 17 the same mean stress correction to the S–N curves was performed as described in Chapter 3.4 for the LNWS results. The low values of  $\delta_b$  and  $K_t$  in SSPPFW (i.e. pillar-to-deck weld) are caused by the un-symmetrical structural arrangement at the fatigue critical location, which is discussed in Chapter 4.

4. Discussion

In steel structures, connections with structural discontinuities causing severe force concentrations along weld seam can appear when the connection is optimised for production in terms of time and costs.

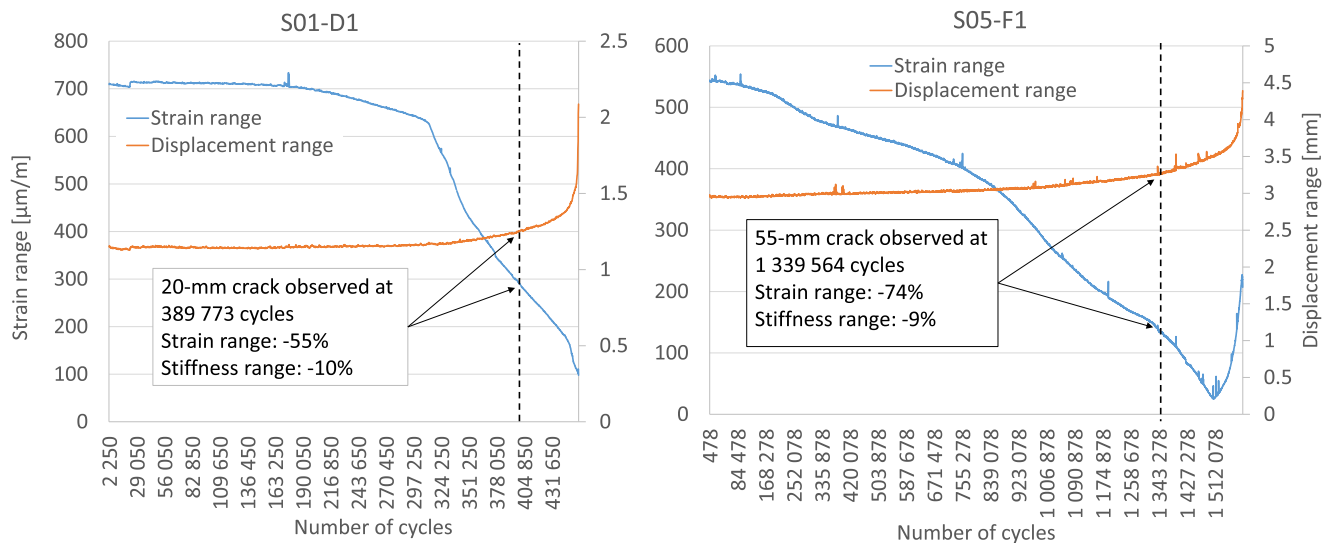


Fig. 13. Examples of strain range and connection stiffness history at fatigue critical location: the RHS-to-deck connection in S01-D1 specimen (left) and the backing plate-to-flange connection in S05-F1 specimen (right).

However, very limited investigations can be found in the literature for full-scale structures with weld root fatigue failure. This problem has received less attention as the focus has typically been on weld toe fatigue; see e.g. [1,3,21]. In the present paper, complex full-scale three-dimensional test specimens with severe force concentrations along the weld length were tested with the fatigue failure at the weld root. The fatigue test results were analysed with local nominal, structural, and effective notch stress approaches; see Table 10. In design codes and recommendations, nominal stress-based analysis uses varying FAT classes depending on the weld and connection type, whereas structural stress and ENS use a fixed FAT class regardless of the connection type. In this respect, the unexpected result of this study was that the LNWS approach resulted in the most accurate fatigue life estimations, with a scatter index of 1.26 to 1.68, depending on the weld type, in comparison to the 4.98 and 5.40 achieved with the structural and ENS approaches respectively.

Using a fixed S–N–curve slope of  $m = 3$ , LNWS was the only approach resulting in a higher characteristic FAT class compared to design codes when both weld types are considered. LNWS resulted in FAT53 for fillet welds and FAT71 for the cases for partial penetration welds. The result for fillet welds is higher than according to the tests by Fricke [9] for an attachment weld end with FAT41. For partial penetration welds, studies with complex connections to be compared with the present paper were not found in the literature.

The structural weld stress approach resulted in FAT44 with all weld types considered, being 45 % lower than given in the design codes, i.e. FAT80. It is noteworthy that the values of the structural stresses were high in some of the specimens, being 685 MPa at the highest, meaning that significant local plasticity was induced at the weld root. All the points below FAT80 had a degree of bending below  $\delta_b = 0.21 \dots 0.47$ , while the points above had a degree of bending  $0.55 \dots 0.71$ . This suggests that the structural weld stress approach results in non-conservative results for welds with a low degree of bending. In the fatigue tests by Fricke [11], the degree of bending was between 0.63 and 0.81 and resulted in a class FAT89.4 with a 97.7 % probability of survival.

The low degree of bending ( $\delta_b = 0.21 \dots 0.47$ ) of single-sided partially penetrating fillet welds (SSPPFW) at the pillar-to-deck connection is caused by the un-symmetrical structural arrangement at the fatigue critical RHS corner. Such an arrangement creates an even force flow through the SSPPFW to the structures below deck, as schematically shown in Fig. 18. In comparison, a schematic representation of the force flow in a symmetrical connection, as in the RHS connection by Fricke [11], is shown where the resultant force is very close to the weld root,

creating a high degree of bending ( $\delta_b = 0.77 \dots 0.81$ ). In the force flux presentation shown in Fig. 18 it is assumed that forces travel from one structural member to another using the shortest route.

It is unexpected that the effective notch stress (ENS) approach resulted in FAT111 with all weld types considered, being 51 % smaller than given in the design codes and with a high scatter range index of 5.40. In the fatigue tests by Krenzel [20] and Fricke [4] a clearly smaller scatter was obtained. The difference from the present paper could be explained by the large variation in the notch stress concentration factor  $K_t$  in the present study, which is because of the widely varying local geometry of the critical area, whereas in Refs. [4,20] this variation was smaller. Fig. 17 shows that the ENS results do indeed depend on the notch stress concentration factor  $K_t$  and values below  $K_t = 2.2$  clearly results in under-conservative fatigue strength with respect to the FAT225 design curve. The low  $K_t$  values are also explained by the even force flow through SSPPFW (see Fig. 18). Similar observations of under-conservative fatigue strength for low  $K_t$  values by Pedersen et al. [27] showed that for a butt-welded connection some points were below FAT225 with  $K_t$  values of between 1.6 and 2.0. Fig. 17 also shows that high values above  $K_t = 5.8$  can lead to clearly under-estimated fatigue life. As shown by Krenzel [20] and Fricke et al. [18,19], some variation to the calculated stress can also be expected from the root geometry and the sub-modelling technique applied. As described in [4–5], the ENS approach with a 1-mm radius is limited to plate thicknesses  $\geq 5$  mm since for thinner plates it may cause problems because of the weakening of the load-carrying cross-section. To overcome this problem 0.3-mm and 0.05-mm notch approaches with specific FAT classes have been created for plates thinner than 5 mm. In the present study keyhole root modelling was applied, and the minimum plate thickness was 5 mm. On the basis of the IIW recommendation limit of  $\geq 5$  mm, the ENS results of this paper are considered to be valid. The 5-mm limit was also fulfilled with most of the weld throat thicknesses at the primary failure location. Only two specimen, i.e. the double fillet welds, had a failed weld throat thickness below 5 mm but their ENS results showed similar behaviour to all the other specimens (see Fig. 17b). The common understanding in engineering is that with complex welded connections failing from the weld root the ENS approach is preferred, as it captures the stress flow through the welds correctly and is therefore the most accurate approach among the stress-based approaches. Therefore, the results from the present paper are relevant observations demonstrating that applying ENS to a complex welded connection can result in unrealistic fatigue life estimations because of very high scatter.

From Table 8 and Table 9 it can be seen that the primary failure

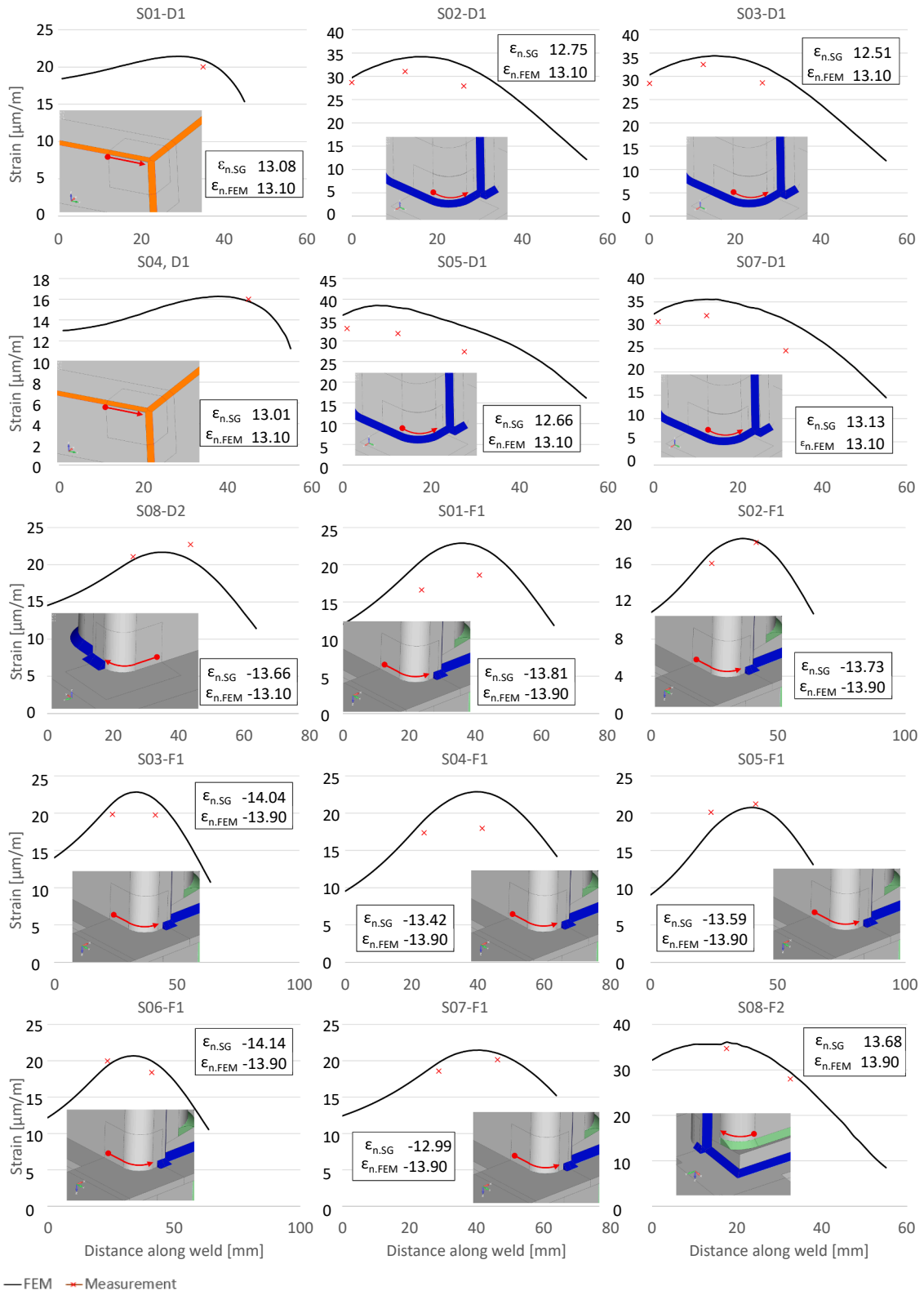


Fig. 14. Strain comparison between the FE model and strain gauge measurements at the primary failure location. Comparison at nominal strain levels shown in the text boxes.

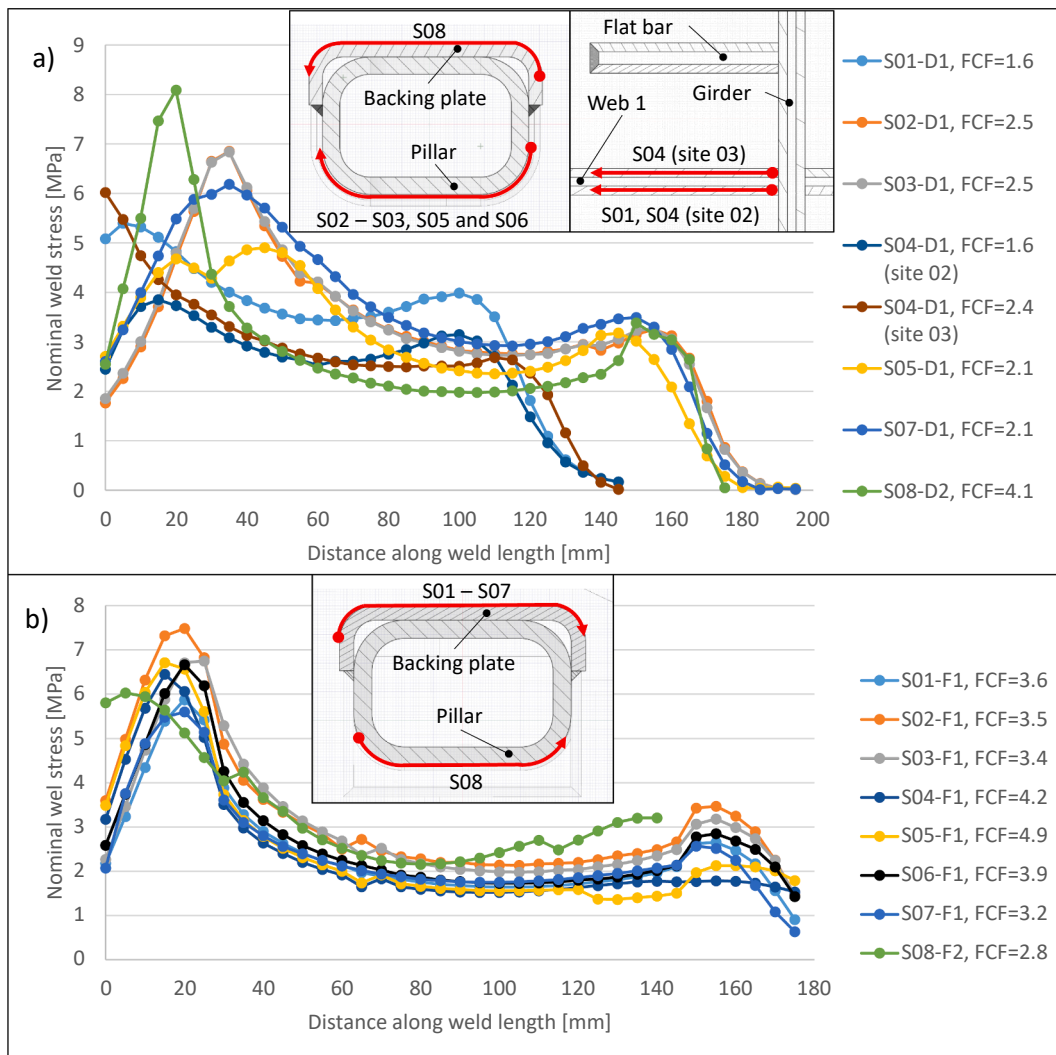


Fig. 15. Nominal weld stress distribution in the failed welds with a 1-kN unit load and force concentration factor (FCF). The corresponding welds and plotting direction are shown in the detail pictures: a) deck connection; b) flange connection.

Table 8

Peak local nominal weld stress [MPa] and degree of bending with a 1-kN unit load. Primary failure location highlighted in green. Test setups D1 and D2.

	Weld no. 4 RHS-deck		Weld no. 5 Web-deck IN		Weld no. 6 Web-deck OUT		Weld no. 1 Backing plate- deck		Weld no. 8 Girder-deck OUT	
	$\sigma_{n,w,loc}$	$\delta_b$	$\sigma_{n,w,loc}$	$\delta_b$	$\sigma_{n,w,loc}$	$\delta_b$	$\sigma_{n,w,loc}$	$\delta_b$	$\sigma_{n,w,loc}$	$\delta_b$
S01-D1	5.9	0.2	6.5	NaN	5.5	0.71	-	-	-	-
S02-D1	6.9	0.34	7.4	NaN	5.4	0.72	-	-	-	-
S03-D1	6.7	0.34	6.5	NaN	4.4	0.70	-	-	-	-
S04-D1	5.7	0.37	6.0	0.64	3.8	0.71	-	-	-	-
S05-D1	4.9	0.29	7.1	0.62	3.5	0.72	-	-	-	-
S07-D1	6.2	0.00	6.5	0.61	4.6	0.69	-	-	-	-
S08-D2	-	-	-	-	-	-	8.3	0.56	6.4	0.70

location was in correlation with the weld that had the highest local nominal stress in the flange connection tests. In a deck connection, on the other hand, the primary failure location is not perfectly in line with the weld that has the highest local nominal stress. On the basis of the stresses shown in Table 5, it is possible that weld no. 5 with the peak stress location at the weld intersection or very close to it, has better resistance to crack propagation because of the weld intersection compared to weld no. 4.

The fatigue test results of this paper can be considered valid for all three local approaches as the definition of the number of cycles for

failure is based on a crack with a length of 20 mm.<sup>3</sup> However, the exact crack length to match with the number of cycles to failure of the rest of the specimens could not be defined as the length of the first observed crack length varied between 20 mm and 187 mm. From the local cracking to the complete failure of the connection there was 1.1 to 1.9

<sup>3</sup> Failure was defined as the number of cycle in which the local strain range was reduced by 55%, which corresponded to a 20-mm visual crack on the S01-D1 test specimens.

**Table 9**

Peak nominal weld stress [MPa] and degree of bending with a 1-kN unit load. Primary failure location highlighted in green. Test setups F1 and F2.

	Weld no. 21 Backing plate-flange		Weld no. 14 FB-flange IN		Weld no. 13 FB-flange OUT		Weld no. 26 RHS-wedge		Weld no. 24 Wedge-flange	
	$\sigma_{n,w,loc}$	$\delta_b$	$\sigma_{n,w,loc}$	$\delta_b$	$\sigma_{n,w,loc}$	$\delta_b$	$\sigma_{n,w,loc}$	$\delta_b$	$\sigma_{n,w,loc}$	$\delta_b$
S01-F1	5.9	0.55	2.9	NaN	3.7	NaN	-	-	-	-
S02-F1	7.4	0.57	3.1	NaN	3.6	0.73	-	-	-	-
S03-F1	6.8	0.52	3.0	NaN	3.9	NaN	-	-	-	-
S04-F1	6.3	0.53	2.5	NaN	5.0	NaN	-	-	-	-
S05-F1	6.7	0.59	1.6	NaN	4.8	0.63	-	-	-	-
S06-F1	6.7	0.59	3.2	NaN	4.6	NaN	-	-	-	-
S07-F1	5.6	0.60	3.4	NaN	3.9	0.73	-	-	-	-
S08-F2	-	-	-	-	-	-	5.8	0.50	5.5	0.56

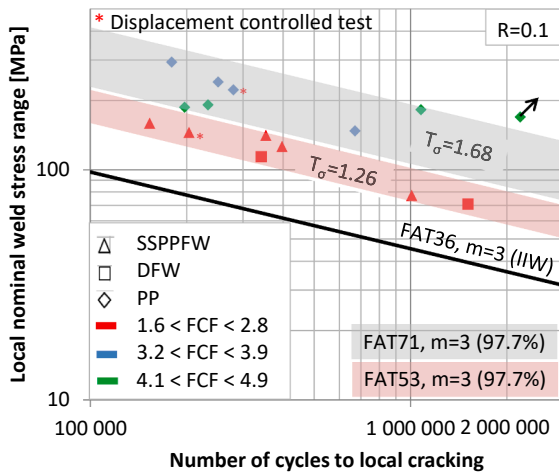


**Fig. 16.** Local nominal weld stress  $S-N$  curve using colour coding according to the force concentration factor FCF. The test points are for a load ratio  $R = 0.1$ , while the calculated characteristic FAT class values are for  $R = 0.5$  to compare them to the IIW FAT class.

times more fatigue life left in the fillet welds with FCF from 1.6 to 2.8. Then again, from the local cracking to the complete failure of the connection there was 1.5 to 3.4 times more fatigue life left in the partial penetration welds with FCF from 3.2 to 4.9. Therefore the specimens with more severe force concentrations had a higher redundancy to complete failure after local cracking.

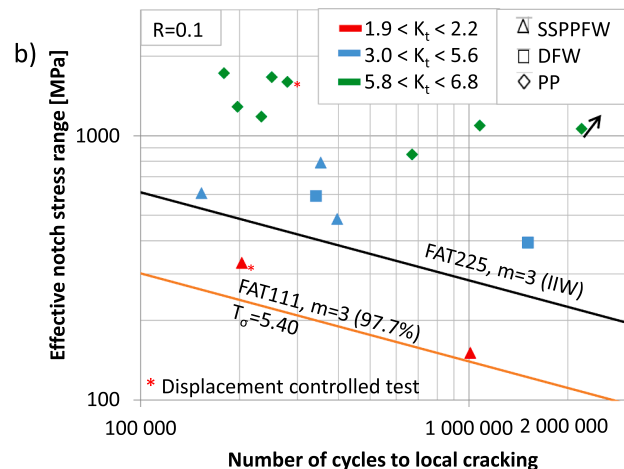
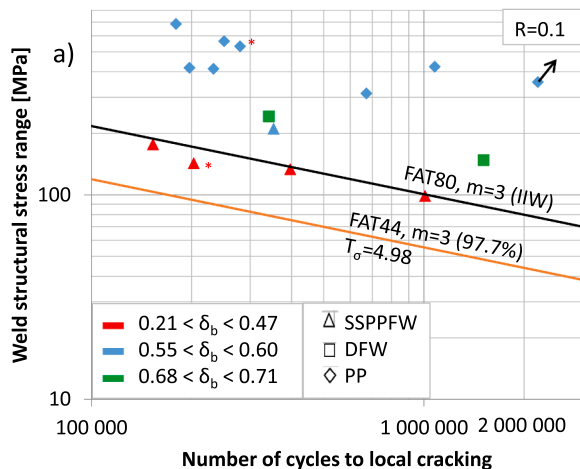


**Fig. 17.** Structural weld stress (a) and effective notch stress  $S-N$  curves (b). The test points are for the load ratio  $R = 0.1$ , while the calculated characteristic FAT class values and  $S-N$  curves are for  $R = 0.5$  to compare them to the IIW FAT class and  $S-N$  curves.

**5. Conclusion**

This paper investigated the weld root fatigue strength of complex welded connections by carrying out fatigue tests for full-scale, three-dimensional pillar connection specimens with severe force concentrations along the weld length. Various details were tested with varying stress concentration factors including fillet welds, partial penetration welds and partially penetrated fillet welds. The results were analysed with three local stress-based approaches: local nominal and structural weld stress and the ENS approach. FE models were created that were based on the geometry measurements. The FE results were validated by comparing the strains with the strain gauge measurements. From this study the following conclusions can be drawn:

**Table 10**

Comparison with LNWS, structural weld stress and ENS approaches.

	LNWS		Weld structural stress		ENS
Weld type	FW	PP	FW and PP	FW and PP	FW and PP
Scatter range index	1.26	1.68	4.98		5.40
FAT class	53	71	44		111
Design FAT class	36	36	80		225
Difference from design curve [%]	+47	+97	-45		-51
FW includes the weld types SSPPFW and DFW.					

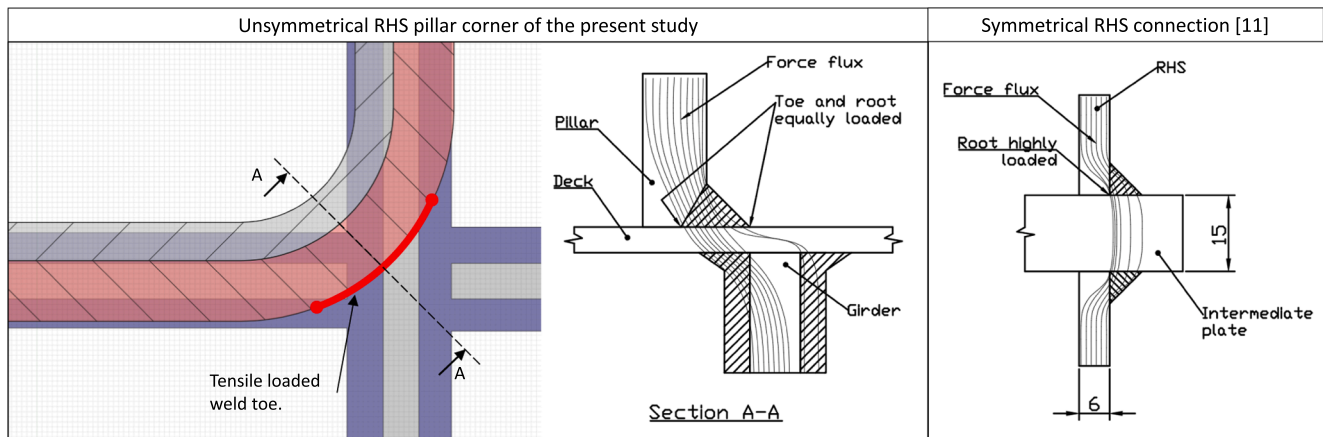


Fig. 18. Force flow through welds in the fatigue critical cross-section of the RHS corner in the un-symmetrical connection of the present paper with single-sided partially penetrating fillet welds (left) and in the symmetrical RHS connection by Fricke with single sided fillet welds [11] (right).

- the fatigue life of welded connections in large complex structures is highly dependent on the weld force concentration factor and stress concentration factor  $K_t$ , on which the weld type can have a significant effect because of varying degrees of bending and the stress gradient at the weld root
- the local nominal weld stress (LNWS) approach seems to suit best the weld root analysis of complex welded connections with varying stress concentrations along the weld seam. LNWS was least affected by the degree of bending or stress concentration, resulting in the lowest scatter
- the structural weld stress approach resulted in an over-estimated fatigue life for welds with a low degree of bending and higher scatter than LNWS
- for an effective notch stress approach, the severity of the stress concentration in a large complex connection causes a very high scatter and can lead to a significantly over- or under-estimated fatigue life with a FAT225 curve.

**Declaration of Competing Interest**

The authors declare that they have no known competing financial interests or personal relationships that could have appeared to influence the work reported in this paper.

**Data availability**

The data that has been used is confidential.

**Acknowledgements**

This research was funded by Meyer Turku Oy. The funding is gratefully appreciated. Sincere thanks to the Aalto University Solid Mechanics laboratory staff for their hard work with the fatigue tests.

**Appendix A**

See Table A1.

**Table A1**  
Test matrix and fatigue test results.

ID	Test setup	FC/DC	Load range [kN]	$N_{loc}$	$N_{final}$	$\Delta\sigma_{n,w,loc}$ [MPa]	$\Delta\sigma_{ws}$ [MPa]	$\Delta ENS$ [MPa]
S01	D1	FC	2.3–23.1	342 250	461 000	113.8	241.4	590.6
S03	F1	FC	2.4–24.1	671 200	1 627 000	147.3	313.1	849.4
S04	F1	FC	3.0–30.0	2 203 538	2 203 538*	169.2	355.5	1061.4
S01	F1	FC	3.6–36.0	233 280	783 080	191.2	413.4	1179.4
S06	F1	FC	4.0–40.0	250 878	529 278	240.8	564.1	1664.3
S05	F1	FC	3.0–30.0	1 078 678	1 600 078	182.1	423.1	1091.9
S02	F1	FC	4.4–44.0	179 570	269 570	293.8	685.2	1722.6
S02	D1	FC	2.58–25.8	153 327	273 327	159.2	176.2	605.3
S03	D1	FC	2.1–21.0	397 003	559 803	126.0	133.4	483.8
S04	D1	FC	1.6–16.0	1 512 903	2 333 103	70.8	147.6	393.6
S05	D1	FC	1.75–17.5	1 009 135	1 473 735	77.2	98.7	150.4
S07	F1	DC	4.4–44.0	280 076	499 876	222.1	532.1	1597.9
S08	F2	FC	2.7–27.0	353 563	381 363	140.9	210.2	791.0
S07	D1	DC	2.6–26.0	203 477	379 877	145.1	142.3	329.7
S08	D2	FC	2.5–25.0	197 348	352 548	186.9	418.4	1285.4

\* Run-out.

## References

- [1] Larsen ML, Arora V, Lützen M, Pedersen RR, Putnam E. Fatigue life estimation of the weld joint in K-node of the offshore jacket structure using stochastic finite element analysis. *Mar struct* 2021;78:103020.
- [2] Baptista C, Kannuna S, Oliveira Pedro J, Nussbaumer A. Fatigue behaviour of CHS tubular bracings in steel bridges. *Int J Fatigue* 2017;96:127–41.
- [3] Fricke W. Full-scale fatigue tests of ship structures to validate the S-N approaches for fatigue strength assessment. *Mar struct* 2010;23(1):115–30.
- [4] Fricke W. IIW guideline for the assessment of weld root fatigue. *Welding World* 2013;57(6):753–91.
- [5] Hobbacher AF. Recommendations for Fatigue Design of Welded Joints and Components. Cham: Springer; 2016.
- [6] Eurocode 3, Design of steel structures, Part 1-9, Fatigue, EN 1993-1-9, Brussels, CEN, 2006.
- [7] DNVGL-RP-C203 Fatigue design of offshore steel structures. 2014.
- [8] Rautiainen M, Remes H, Niemelä A. A traction force approach for fatigue assessment of complex welded structures. *Fatigue Fract Eng Mater Struct* 2021;44(11):3056–76.
- [9] Fricke W, Doerk O. Simplified approach to fatigue strength assessment of fillet-welded attachment ends. *Int J Fatigue* 2006;28(2):141–50.
- [10] Sorensen J, Tychsen J, Andersen J, Brandstrup R. Fatigue analysis of load-carrying fillet welds. *J Offshore Mech Arct Eng* 2006;128(1):65–74.
- [11] Fricke W. Fatigue Assessment of Root Cracking of Fillet Welds Subject to Throat Bending using the Structural Stress Approach. *Welding in the World* 2006;50(7):64–74.
- [12] Meneghetti G, Guzzella C, Atzori B. The peak stress method combined with 3D finite element models for fatigue assessment of toe and root cracking in steel welded joints subjected to axial or bending loading. *Fatigue Fract Eng Mater Struct* 2014;37(7):722–39.
- [13] Wang P, Pei X, Dong P, Song S. Traction structural stress analysis of fatigue behaviors of rib-to-deck joints in orthotropic bridge deck. *Int J Fatigue* 2019;17:11–22.
- [14] Foti P, Berto F. Fatigue assessment of high strength welded joints through the strain energy density method. *Fatigue Fract Eng Mater Struct* 2020;43(11):2694–702.
- [15] Frank D, Remes H, Romanoff J. J-integral-based approach to fatigue assessment of laser stake-welded T-joints. *Int J Fatigue* 2013;47:340–50.
- [16] Radaj D, Sonsino C, Fricke W. Fatigue Assessment of Welded Joints by Local Approaches. 2nd ed. Cambridge: Woodhead Publishing; 2006.
- [17] Baumgartner J. Review and considerations on the fatigue assessment of welded joints using reference radii. *Int J Fatigue* 2017;101:459–68.
- [18] Fricke W, Bollero A, Chirica I, Garbatov Y, Jancart F, Kahl A, et al. Round robin study on structural hot-spot and effective notch stress analysis. *Ships Offshore Struct* 2008;3(4):335–45.
- [19] Fricke W, Codda M, Feltz O, Garbatov Y, Remes H, Risso G, et al. Round robin study on local stress and fatigue assessment of lap joints and doubler plates. *Ships Offshore Struct* 2013;8(6):621–7.
- [20] Krenzel M. Fatigue Strength of a Welded Tube-to-Plate Joint at an Offshore Structure [dissertation]. University of Southern Denmark; 2019.
- [21] Lillemäe I, Liinalampi S, Remes H, Itävuo A, Niemelä A, Department of Mechanical E, et al. Fatigue strength of thin laser-hybrid welded full-scale deck structure. *Int J Fatigue* 2017;95:282–292.
- [22] GOM ATOS 3D Scanner System 3D Blue Optical Light, <https://pes-scanning.com/3d-scanning-technology/gom-atos-3d-scanner> [accessed: 14 June 2022].
- [23] ANSYS SpaceClaim, <https://www.ansys.com/products/3d-design/ansys-spaceclaim> [accessed: 14 June 2022].
- [24] Femap User Guide Version 11.4.2.
- [25] NX Nastran 11.0.2 Release Guide.
- [26] Sonsino CM. A Consideration of allowable equivalent stresses for fatigue design of welded joints according to the notch stress concept with the reference Radii  $r_{ref} = 1.00$  and  $0.05$  mm. *Welding World* 2009;53(3):R64–75.
- [27] Pedersen MM, Mouritsen OØ, Hansen MR, Andersen JG, Wenderby J. Re-analysis of fatigue data for welded joints using the notch stress approach. *Int J Fatigue* 2010;32(10):1620–6.